Applied Catalysis B: Environmental 332 (2023) 122746

Contents lists available at ScienceDirect

Applied Catalysis B: Environmental

journal homepage: www.elsevier.com/locate/apcatb

Direct synthesis of high silica SSZ-16 zeolite with extraordinarily superior performance in NH_3-SCR reaction

Shichao Han [a,b,1], Wei Rao [c,1], Junyi Hu [d,1], Xiaomin Tang [c], Ye Ma [d], Jinpeng Du [a,b], Zhongqi Liu [e], Qinming Wu [f], Yanhang Ma [d], Xiangju Meng [g], Wenpo Shan [a,b,*], Feng-Shou Xiao [f,**], Hong He [a,e]

[a] Center for Excellence in Regional Atmospheric Environment, Institute of Urban Environment, Chinese Academy of Sciences, Xiamen 361021, PR China
[b] Zhejiang Key Laboratory of Urban Environmental Processes and Pollution Control, Ningbo Urban Environment Observation and Research Station, Institute of Urban Environment, Chinese Academy of Sciences, Ningbo 315800, PR China
[c] State Key Laboratory of Magnetic Resonance and Atomic and Molecular Physics, National Center for Magnetic Resonance in Wuhan, Key Laboratory of Magnetic Resonance in Biological Systems, Wuhan Institute of Physics and Mathematics, Innovation Academy for Precision Measurement Science and Technology, Chinese Academy of Sciences, Wuhan 430071, PR China
[d] School of Physical Science and Technology & Shanghai Key Laboratory of High-resolution Electron Microscopy, ShanghaiTech University, Shanghai 201210, PR China
[e] State Key Joint Laboratory of Environment Simulation and Pollution Control, Research Center for Eco-Environmental Sciences, Chinese Academy of Sciences, Beijing 100085, PR China
[f] College of Chemical and Biological Engineering, Zhejiang University, Hangzhou 310027, PR China
[g] Key Lab of Applied Chemistry of Zhejiang Province, Department of Chemistry, Zhejiang University, Hangzhou 310007, PR China

ARTICLE INFO

Keywords:
High silica
SSZ-16 zeolite
Diquaternary alkylammonium
Hydrothermal stability
NH_3-SCR

ABSTRACT

The development of Cu ion-exchanged small-pore zeolites with excellent performance and high hydrothermal stability in NH_3-SCR reaction is of great importance. However, many frameworks of the small-pore zeolites are Al-rich, for instance, Cu-SSZ-16 zeolite with Si/Al ratio always no more than 5, showing relatively low hydrothermal stability. In this work, inspired by theoretical calculation for the interaction between organic structural directing agents (OSDAs) and zeolite framework, high silica SSZ-16 zeolite with Si/Al ratio at 6.7 was directly synthesized using an economical diquaternary alkylammonium cation as an OSDA. After exchanged with Cu ion, the Cu-SSZ-16 catalyst shows extraordinarily superior performance in NH_3-SCR reaction even after hydrothermal aging at 900 °C. The designed synthesis combined with excellent performance as well as high hydrothermal stability of the high silica SSZ-16 zeolite might provide an attractive alternative candidate for NH_3-SCR catalyst on diesel vehicles and non-road mobile machinery in the future.

1. Introduction

Cu ion-exchanged small-pore zeolites with superior activity, high hydrothermal stability, and good poisoning resistance were studied extensively for selective catalytic reduction of nitrogen oxides (NO_x) with ammonia (NH_3-SCR) [1–8], especially for Cu-SSZ-13 catalyst, which has been commercially applied on diesel vehicles worldwide [9–15]. However, this catalyst shows a striking decrease of deNO_x activity after hydrothermal aging at 850 °C. Other small-pore zeolite catalysts like Cu-SSZ-39 and Cu-LTA show higher hydrothermal stability, in particular with Cu-LTA having good NO_x conversion even after hydrothermal aging at 900 °C. Nevertheless, the requirements of expensive organic structure directing agents (OSDAs) or toxic F^- in the synthetic process of Cu-SSZ-39 or Cu-LTA limit their wide applications [2,16–19]. Therefore, the development of green and sustainable synthesis of small-pore zeolites with superior hydrothermal stability is of great importance for industrial application in the NH_3-SCR.

SSZ-16 zeolite with AFX topology has a three-dimensional microporous structure constructed by the AABBCCBB sequence of *d6r* [20,21]. Its similar framework structure to SSZ-13 led SSZ-16 to be looked upon

* Corresponding author at: Center for Excellence in Regional Atmospheric Environment, Institute of Urban Environment, Chinese Academy of Sciences, Xiamen 361021, PR China.
** Corresponding author.
E-mail addresses: wpshan@iue.ac.cn (W. Shan), fsxiao@zju.edu.cn (F.-S. Xiao).
[1] S. C. Han, W. Rao and J. Y. Hu contributed equally.

https://doi.org/10.1016/j.apcatb.2023.122746
Received 28 February 2023; Received in revised form 3 April 2023; Accepted 6 April 2023
Available online 7 April 2023

as one of the few equivalents to SSZ-13 zeolite for NH_3-SCR reaction [22,23]. However, the relatively low Si/Al ratio of Cu-SSZ-16 catalyst results in poor hydrothermal stability, which hinders its application in NH_3-SCR for NO_x emission control [24–26]. For example, Cu-SSZ-16 catalyst with Si/Al ratio no more than 4 generally lost its structure after hydrothermal aging at 800 °C [27]. Recently, Tatsushi et al. reported a post-synthetic approach to tune the composition of small-pore zeolites, obtained dealuminated SSZ-16 zeolite with the Si/Al ratio at 9.3, which showed excellent NO_x conversion even after hydrothermal treatment at 800 °C for 7 h [28]. This result clearly verified that improving Si/Al ratio of SSZ-16 zeolite is an efficient route to enhance its hydrothermal stability. However, the post-synthetic dealumination process is rather complicated and energy consuming, which still hinders its industrial application.

As for direct synthesis of high silica SSZ-16 zeolite, great efforts have been applied to develop appropriate OSDAs. For example, Okubo et al. successfully synthesized SSZ-16 zeolite with the Si/Al ratio at 4.66 by employing N,N,N′,N′-tetraethylbicyclo[2.2.2]oct-7-ene-2,3,5,6-dipyrrolidinium as an OSDA, and the products they obtained could maintain its structure and showed excellent NO_x conversion after hydrothermally aged at 800 °C for 5 h [27]. Apart from this, other OSDAs like 1,3-bis (1-adamantyl)imidazolium [29] and some bulky and rigid dicationic organic molecules [30] were also used to synthesize high silica SSZ-16. With these complex and expensive OSDAs, however, the Si/Al ratios of most reported SSZ-16 zeolites are still less than 5, which could not significantly improve the hydrothermal stability of SSZ-16 zeolite. Therefore, it still has a great challenge to directly synthesize high silica SSZ-16 zeolite with superior hydrothermal stability.

The pore structure of AFX is formed by *aft* cages (0.55 × 1.35 nm), which are 40 % longer than the *cha* cages in the SSZ-13 zeolite, and *gme* cages (0.33 × 0.74 nm), which are always occupied by inorganic SDAs [31] (Fig. 1). This structure led SSZ-16 to be synthesized with OSDAs in long and narrow shapes, such as 1,4-bis(1-azoniabicyclo[2.2.2]-octane) butyl (Dab-4^{2+}) [21] and 1,3-Bis(1-adamantyl)imidazolium [29]. Considering that diquaternary alkylammonium cations are a common kind of OSDAs which are more flexible and lower cost than those bicyclic OSDAs, in this work, we proposed diquaternary alkylammonium cations with different length of linear and branched carbon chains as OSDAs for the synthesis of high silica SSZ-16 zeolite. Through modeling of interaction between these OSDAs and SSZ-16 zeolite structure [32,33], we successfully synthesized pure SSZ-16 zeolite with two suitable small molecules: N,N′-dimethyl-N,N,N′,N′-tetraethylpentanediyl diammonium (Et_4Me_2-diquat-5), and N,N′-dimethyl-N,N,N′, N′-tetraethylhexanediyldiammonium (Et_4Me_2-diquat-6). Among these small molecules, the Si/Al ratio of the SSZ-16 product obtained with Et_4Me_2-diquat-6 as the OSDA is about 6.7. Very interestingly, after ion exchanged with Cu^{2+}, the Cu-SSZ-16 catalyst showed excellent performance in the NH_3-SCR reaction even after hydrothermal treatment at 850 °C for 16 h and 900 °C for 4 h, which has much higher hydrothermal stability than that of conventional Cu-SSZ-16 catalysts with Si/Al ratio at 3.0 and even those of Cu-SSZ-13 catalysts with Si/Al ratio at 6.8. The combination of designed synthesis and excellent catalytic performance of SSZ-16 zeolite might provide a new generation, highly efficient, and low-cost NH_3-SCR catalysts in the future.

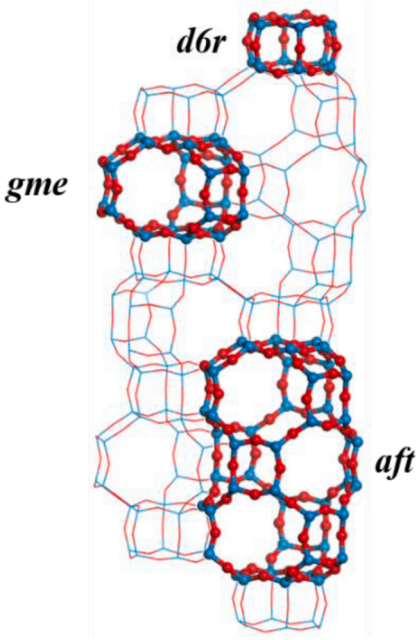

Fig. 1. Structure of AFX framework and its building units.

2. Experimental

2.1. Computational method

Crystal structure of AFX zeolite was taken from the International Zeolite Association [34], and then optimized. Subsequently, a 2 × 2 × 2 supercell was made, where 16 no. of OSDA molecules were placed manually, and AFX_OSDA structure was also optimized. The molecular dynamics (MD) simulations about AFX, AFX_OSDA and OSDA were performed for 30 ps equilibration and 5 ps production with a timestep of 1 fs at 160 °C. The reported energy values of AFX, AFX_OSDA and OSDA were the average energy calculated from the production process. The DREIDING force field [35] was applied to all the optimization and MD simulations in GULP software [36]. According to Deem's method [37], the stabilization energy can be defined as the energy difference between AFX_OSDA, AFX and OSDA in the following:

$$E(\text{stabilization energy}) = [E(\text{AFX\_OSDA}) - E(\text{AFX}) - nE(\text{OSDA})]/\ N$$

Where n refers to the number of OSDA, which equals to 16 in this work; N is the number of T sites in AFX zeolite, which is 384.

The shape of OSDA can be described by a cuboid box. Therefore, the length, width, and height of box can represent the molecular size. To achieve the geometry optimization of OSDAs, the calculations have been carried out at the B3LYP/6-31 g(d) level using Gaussian 09 package [38]. Based on the improved marching tetrahedra algorithm, the Multiwfn version 3.5 software was empolyed to get the volume and size with electron density isosurface set as 0.001 a.u. [39,40].

2.2. Zeolite synthesis

In the synthesis of Et_4Me_2-diquat-6 cation, 24.4 g of 1,6-dibromohexane and 21.8 g of N,N-diethylmethylamine were dissolved in 250 mL acetonitrile, stirring for 24 h under reflux. After cooling to room temperature, the solid product after filtration was washed with anhydrous ether and dried under vacuum overnight. The bromide cations were converted to hydroxide form using hydroxide exchange resin in water, and the concentration of the Et_4Me_2-diquat-6 solution was titrated by HCl standard solution.

In a typical run for the synthesis of high silica SSZ-16 zeolite, 0.1 g of NaOH and 1 g of FAU zeolite (Si/Al=13) was added in a clear solution with 5.56 g of $R(OH)_2$ (0.75 M) and 7.67 g of H_2O. After stirring for 5 h, an aluminosilicate gel with a molar ratio at 1.0 Al_2O_3 / 26.0 SiO_2 / 1.3 Na_2O / 6.5 $R(OH)_2$ / 1040 H_2O was obtained and then transferred to a Teflon-lined autoclave oven and crystallized at 160 °C for 60 h under static condition. After filtration with a large amount of water, the product was dried at 110 °C overnight, and the yield of the high silica SSZ-16 product was 66 %.

2.3. Preparation of catalysts

As-synthesized high silica SSZ-16 zeolite was calcined at 600 °C for 5 h in air to remove the OSDA, following by ion exchange with 1 M NH_4Cl solution for three times to form NH_4-SSZ-16 zeolite. H-SSZ-16 zeolite was then obtained after calcination at 500 °C for 4 h. After exchanging NH_4-SSZ-16 zeolite with 0.05 M $Cu(NO_3)_2$ solution at 40 °C for 6 h, washing, drying and calcinating at 600 °C for 5 h, Cu-SSZ-16 catalyst with copper loading of 2.93 wt% was finally obtained.

As a comparison, conventional SSZ-16 zeolite with the Si/Al ratio at 3.0 was synthesized in the presence of Dab-4^{2+} as reported in the literature,[21] designated as SSZ-16-con. As mentioned above, the product was calcined, and ion exchanged with 1 M NH_4Cl solution. Cu-SSZ-16-con with copper loading of 3.03 wt% was subsequently obtained by ion exchanged with 0.01 M $Cu(NO_3)_2$ solution at 40 °C for 6 h, followed by washing, drying and calcination.

SSZ-13 zeolite with the Si/Al ratio at 6.8 synthesized in the presence of N,N,N-trimethyl-1–1-adamantammonium (TMAdaOH) was also used as a comparison.[41] Cu-SSZ-13 catalyst with copper loading of 2.95 wt % was prepared by NH_4-SSZ-13 ion exchanged with 0.01 M $Cu(NO_3)_2$ solution at 40 °C for 6 h, followed by washing, drying and calcination.

2.4. NH_3-SCR activity test

The catalysts were pressured, crushed, sieved into 40–60 mesh. Catalytic activities in NH_3-SCR reaction were conducted in a fixed-bed quartz flow reactor at atmospheric pressure. The total flow rate was held at 500 mL/min, with gas composition of 500 ppm of NO, 500 ppm NH_3, 5 % H_2O, 5 % O_2, and N_2 as a balance gas (GHSV=200000 h^{-1}). The gas compositions were monitored by an online Nicolet IS50 spectrometer. And then, the NO_x conversion was calculated based on the formula as following:

$$\mathrm{NO}x\mathrm{conversion} = \left(1 - \frac{[NOx]_{out}}{[NOx]_{in}}\right) \times 100\% (NOx = NO + NO_2)$$

The hydrothermal aging of Cu-SSZ-16, Cu-SSZ-16-con and Cu-SSZ-13 catalysts was conducted in flowing air containing of 10 vol% H_2O at 800 °C (HTA800) and 850 °C (HTA850) for 16 h, and 900 °C (HTA900) for 4 h, respectively.

3. Results and discussion

Diquaternary alkylammonium cations with different length were a common series of OSDAs used for the synthesis of different type zeolites such as ZSM-5, ZSM-11, NU-87, ZSM-12 [42–44]. Here, we chose diquaternary alkylammonium cations with different length of linear and branched carbon chains as candidates for the synthesis of high silica SSZ-16 zeolite. Firstly, we performed a computational simulation of the stabilization energies between the AFX framework and a series of diquaternary alkylammonium cations, and compared with these conventional bicyclic OSDAs (Table S1). Considering the balance of preparation method, cost, and interaction stabilization energies, Et_4Me_2-diquat-5 and Et_4Me_2-diquat-6 with relatively low interaction stabilities (−10.94 and −10.86 kJ/mol·Si, respectively, Fig. 2) could be regarded as suitable OSDAs for the synthesis of SSZ-16 zeolite. Secondly, from the concept of charge density mismatch in zeolite crystallization [45], we calculated the volumes of Et_4Me_2-diquat-6 and Dab-4^{2+}, showing that the volume of Et_4Me_2-diquat-6 is larger than Dab-4^{2+} (Table 1), which also suggests that Et_4Me_2-diquat-6 might be an appropriate OSDA for synthesizing high silica SSZ-16 zeolite. In addition, the low Si/Al ratio of the SSZ-16 product synthesized with Dab-4^{2+} as the OSDA might be partially resulted from the presumable existence of protonated Dab-4^{2+} [46].

To confirm the above possibility, synthetic conditions for SSZ-16 zeolite with Et_4Me_2-diquat-5 and Et_4Me_2-diquat-6 as OSDAs were

Table 1
The volume of OSDAs.

OSDA	Et_4Me_2-diquat-6	Dab-4^{2+}
Volume (Å^3)	441.9	427.4
Length (Å)	17.26	20.88
Width (Å)	9.23	8.84
Height (Å)	8.10	7.08

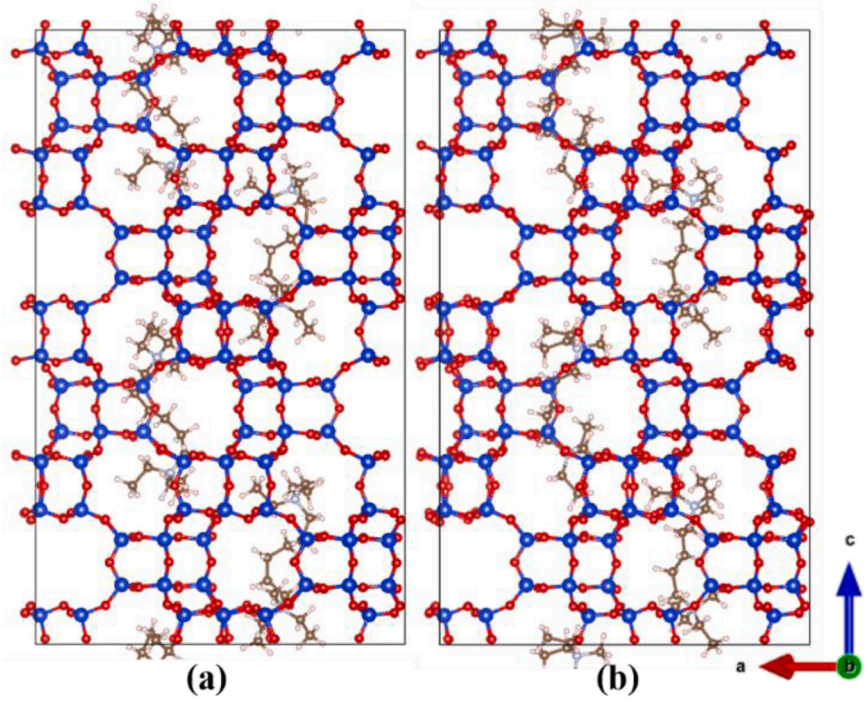

Fig. 2. Positions of (a) Et_4Me_2-diquat-6, and (b) Et_4Me_2-diquat-5 molecules within AFX framework.

optimized. Take the synthesis of SSZ-16 zeolite with Et_4Me_2-diquat-6 for example, it is found that the ratios of Si/Al, Na_2O/SiO_2, and $R(OH)_2/SiO_2$ in the starting gel are critical for the crystallization of SSZ-16 zeolite. As reported, FAU zeolite was an appropriate starting material used for synthesis of many small-pore zeolites, especially those of the ABC-6 family including CHA, ERI and AFX, for that they possessed a common secondary building unit (*d6r*) [47–49]. Martín et al. further proved the importance of this structure similarity for the efficient synthesis of SSZ-16 zeolite [30]. In contrast, the use of colloidal silica as a silica source under the same conditions could not form SSZ-16 but *BEA phase. In addition, interzeolite conversion have been proved to be an efficient method to synthesize high silica small-pore zeolites [50]. In this work, FAU with different Si/Al ratios were used as initial silicon and aluminum sources to synthesize SSZ-16 zeolite. Notably, when the Si/Al ratio of FAU was 13, pure SSZ-16 zeolite with high crystallinity was obtained (Table S2, run 1, Fig. S1a). Once FAU with higher Si/Al ratio of 16 was used, FAU was still observed in the final product (Table S2, run 2, Fig. S1b). Further increasing the Si/Al ratio of FAU to 30, FAU tended to be transferred to MFI phase (Table S2, run 3, Fig. S1c). Additionally, Na_2O/SiO_2 ratio in the gel is an important factor in the crystallization. It was found that pure SSZ-16 zeolite phase was only obtained in a relatively narrow range of Na_2O/SiO_2 ratio from 0.075 to 0.1; too low, the raw material FAU still existed (Table S2, run 4, Fig. S2a); too high, dense phase analcime (ANA) was observed and gradually became the dominant phase (Table S2, run 5–6, Figs. S2b-c). Moreover, when the R $(OH)_2/SiO_2$ ratio in the starting gel was 0.25–0.3, pure SSZ-16 zeolite was obtained; when the $R(OH)_2/SiO_2$ ratio increased to 0.35, FAU was dominant in the final product (Table S2, run 7, Fig. S3a); further increased to 0.4, ANA phase was appeared (Table S2, run 8, Fig. S3b) and dominant in the final product when the ratio was higher than 0.6 (Table S2, run 9, Fig. S3c). Thus, the pure phase of SSZ-16 zeolite could be successfully achieved by optimization of synthetic conditions. As expected, pure SSZ-16 product with Si/Al ratio of 5.8 could also be obtained with Et_4Me_2-diquat-5 as the OSDA (Fig. S4).

Fig. 3 shows characterization results of the SSZ-16 product synthesized with Et_4Me_2-diquat-6. XRD patterns of the as-synthesized and H-formed samples give a series of characteristic peaks associated with the AFX structure (Fig. 3 A). The XRD Rietveld refinement for the sample using the program MAUD further confirms that the product is a pure AFX phase with high crystallinity (Figure 3B, R_p =0.068 and R_{exp}=0.0233). SEM images of the sample show uniform di-hexahedron morphology with the size of 1 μm (Fig. 3C-D). N_2 sorption isotherms of the H-formed sample, as shown in Fig. 3E, gives a typical Langmuir-type curve with BET surface area and micropore volume of 614 m^2/g and 0.22 cm^3/g respectively, comparable to those of the conventional SSZ-16 zeolite synthesized with Dab-4^{2+} [21,27]. Fig. 3 F displays the TG-DTA curves of the as-synthesized sample, showing a weight loss of 14.8 wt% at 300–700 °C attributed to the decomposition of the Et_4Me_2-diquat-6 in the zeolite micropore. Fig. 3 G exhibits ^{13}C NMR spectra of the as-synthesized sample and the Et_4Me_2-diquat-6. Both spectra show similar signal peaks, demonstrating that the Et_4Me_2-diquat-6 exists in the zeolite micropores stably.

Fig. 3H shows ^{27}Al MAS NMR spectrum of the as-synthesized sample, giving a chemical shift at 57.2 ppm associated with coordinated

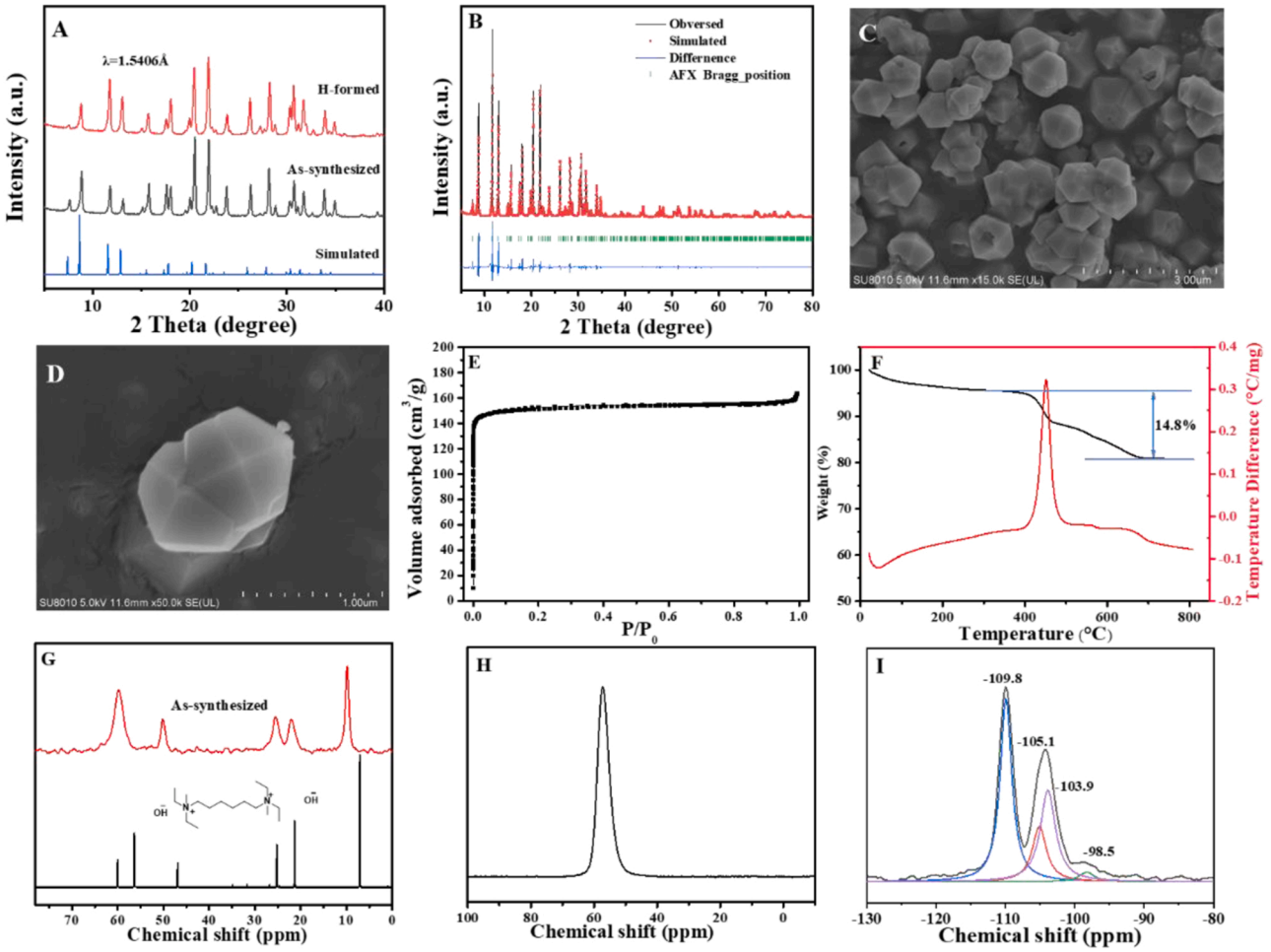

Fig. 3. (A) XRD patterns, (B) Rietveld refinement of the XRD pattern, (C, D) SEM images, (E) N_2 sorption isotherms, (F) TG-DTA curves, (G) ^{13}C NMR, (H) ^{27}Al, and (I) ^{29}Si MAS NMR spectra of high silica SSZ-16 zeolite.

tetrahedral aluminum species in the zeolite framework. At the same time, there is no obvious peak at 0 ppm, revealing the absence of extra-framework aluminum species in the sample. The ^{29}Si MAS NMR spectrum of the as-synthesized sample has four peaks at − 109.8 ppm assigned to Si(4Si), − 105.1 and − 103.9 ppm assigned to Si(3Si) species, and − 98.5 ppm assigned to Si(2Si) species. Through the area of Si (nSi) species obtained after deconvolution (Table S3), it is estimated that the Si/Al ratio of the as-synthesized product is at 7.2 [51], which is in good agreement with the value of 6.7, measured by inductively coupled plasma (ICP) technique. These results demonstrate the successful synthesis of high silica SSZ-16 zeolite in the presence of the Et_4Me_2-diquat-6.

To verify the structure of the high silica SSZ-16 zeolite obtained, selected-area electron diffraction (SAED) and high-resolution transmission electron microscopy (HRTEM) were employed for characterizing as-synthesized SSZ-16 zeolite. Fig. 4 shows the SAED patterns and corresponding HRTEM images that were collected along the [100], [001], and [101] zone axes, respectively. Remarkably, all three projections show excellent agreement with the structural model of the AFX zeolite framework as reported by the International Zeolite Association [34]. These results provide evidence for the successful synthesis of AFX zeolite with high crystallinity.

Crystallization of SSZ-16 zeolite was investigated by XRD and SEM techniques (Figs. S5–S6). When crystallization time is less than 12 h, FAU was dominant in the product (Figs. S5a and S6a). When increasing the crystallization time to 14 h, weak peaks associated with SSZ-16 zeolite appeared (Figs. S5b and S6b). Further increasing the crystallization time from 16 to 48 h, the intensity of the XRD peaks related to SSZ-16 zeolite gradually increased along with the decrease of intensity of the peaks relatedto FAU zeolite (Figs. S5c-g). SSZ-16 zeolite with good crystallinity and perfect di-hexahedron particles could be observed after crystallized for 48 h (Fig. S6g), and no obvious change of the XRD peaks related to SSZ-16 zeolite could be found after further increasing the crystallization time to 60 h, indicating that the sample has been fully crystallized (Figs. S5h and S6h). The dependence of SSZ-16 zeolite crystallinity on time is shown in Fig. S7.

MAS NMR, and UV-Raman techniques were further used to investigate the interzeolite conversion of FAU to AFX zeolite, as shown in Fig. 5. ^{27}Al MAS NMR spectra of the samples crystallized at various time exhibit a transition of signal from the chemical shift at 60.7 to 57.6 ppm (Fig. 5 A), associated with 4-coordinated aluminum in FAU and AFX structure, respectively, indicating that a large fraction of ordered aluminosilicate fragments retained during the dissolution of FAU structure and reassembled to the AFX structure. Fig. 5B gives ^{29}Si MAS NMR spectra of the samples. Before interzeolite transformation, FAU was dominant in the final product, showing three peaks at − 106.5, − 101.4, and − 94.4 ppm which are assigned to Si(4Si), Si(3Si), and Si (2Si) species in FAU structure, respectively. During the crystallization, the intensity of the peaks assigned to the Si(3Si) and Si(2Si) species in FAU zeolite gradually decreased with the increase of the peaks at − 110.5 and − 104.9 ppm, which are associated with Si(4Si) and Si(3Si) species in AFX structure, respectively. These results suggest that during the crystallization, FAU framework was decomposed into ordered aluminosilicate fragments that then built up the framework of AFX.

Fig. 5C shows UV-Raman spectra of the products crystallized at various time. In the initial 12 h, there are three main Raman bands: the band at 312 cm^{-1} is attributed to the bending mode of *d6r* [52,53], while the bands at 488 and 513 cm^{-1} are assigned to the breathing mode vibration of *s4r* in the FAU framework [54,55]. After increasing crystallization time to 16 h, a new Raman band appeared at 333 cm^{-1} in accordance with the appearance of the weak XRD peaks associated with AFX framework. This novel band is related to *d6r* in AFX framework, and this band intensity is strengthened with crystallization time, accompanied with the decrease of the band at 312 cm^{-1}. These results indicate that the *d6r* units in FAU framework stably retained and transformed to AFX framework during the crystallization process. At the same time, the

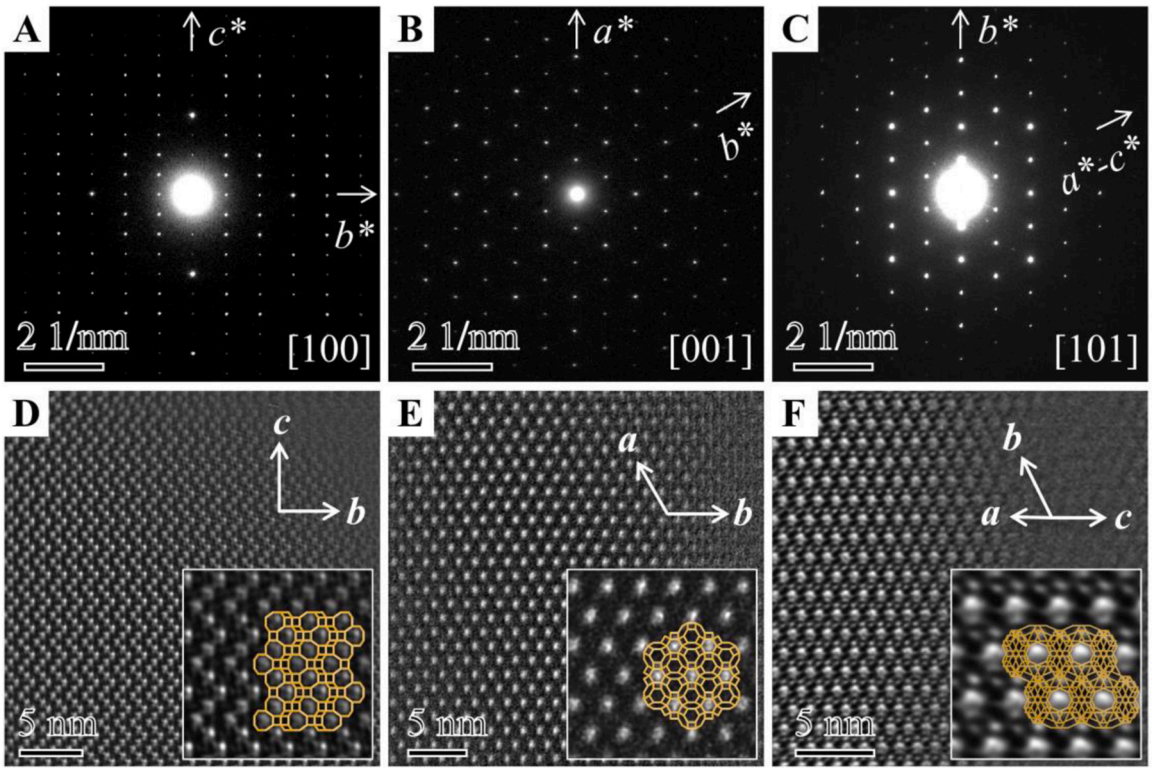

Fig. 4. SEAD patterns and corresponding HRTEM images of high silica SSZ-16 zeolite taken along the (A, D) [100], (B, E) [001], and (C, F) [101] zone axes, respectively. The insert on the bottom right corner is the enlarged images overlaid with the structural models of AFX zeolite showing good agreement. The framework O atoms are omitted for clarity.

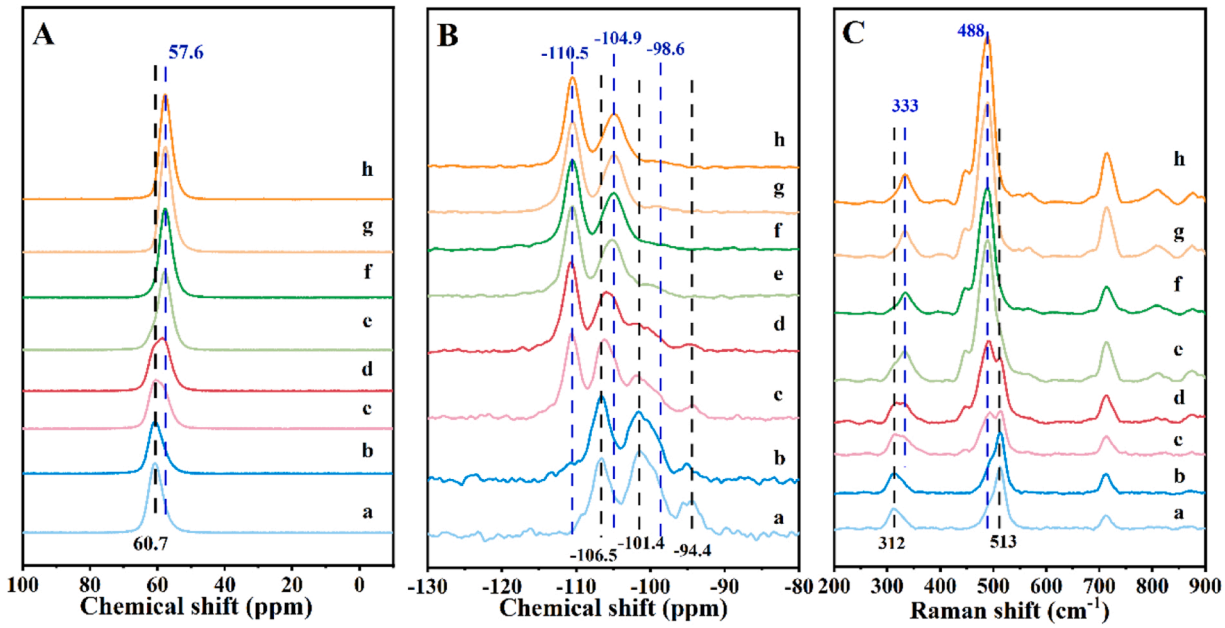

Fig. 5. (A) ^{27}Al, (B) ^{29}Si MAS NMR, and (C) UV-Raman spectra of high silica SSZ-16 zeolite crystallized for (a) 12, (b) 14, (c) 16, (d) 18, (e) 20, (f) 36, (g) 48, and (h) 60 h, respectively.

band at 488 cm^{-1} gradually increased with the reduction of band intensity at 513 cm^{-1}, indicating a successful transfer of *s4r* units from FAU to AFX framework. Therefore, these results support efficient interzeolite transformation between FAU and AFX shared with the same composite building units of *d6r*, which is well consistent with that reported previously for the interzeolite transformations between FAU to CHA and AEI zeolite [47,56–58].

Fig. 6 shows NO_x conversion of fresh and hydrothermally aged Cu-SSZ-16, Cu-SSZ-16-con, and Cu-SSZ-13 catalysts, as a function of temperature from 150° to 550°C under a GHSV of 200000 h^{-1}. Before hydrothermal aging, the fresh Cu-SSZ-13 showed higher NO_x conversion than both of the AFX type catalysts at temperatures below 250 °C. In contrast, at temperatures above 350 °C, Cu-SSZ-16 exhibited similar activity to Cu-SSZ-16-con and both higher than Cu-SSZ-13. After hydrothermal aging at 800 °C, the NO_x conversion of Cu-SSZ-13 decreased slightly, and the activity of Cu-SSZ-16-con lost totally, while Cu-SSZ-16 still showed similar high deNO_x activity as that of the fresh one, indicating that the high silica SSZ-16 possesses remarkably improved hydrothermal stability, compared to Al-rich analogs. The difference between different topology of CHA and AFX was more pronounced after hydrothermal aging at 850 °C. In this case, Cu-SSZ-16 showed NO_x conversions above 80 % within the temperature range of 200–450 °C, while Cu-SSZ-13 completely lost its activity. Clearly, the developed high silica Cu-SSZ-16 was more resistant to hydrothermal aging than Cu-SSZ-13. Further increasing the hydrothermal treatment temperature to 900 °C, the Cu-SSZ-16 still maintain high NO_x conversion (above 80 % within the temperature range of 225–450 °C) after aging for 4 h. The above results clearly indicate that the increase of Si/Al ratio remarkably improves the hydrothermal stability of the AFX framework for SSZ-16 zeolite, making it even more stable than Cu-SSZ-13 with similar Si/Al

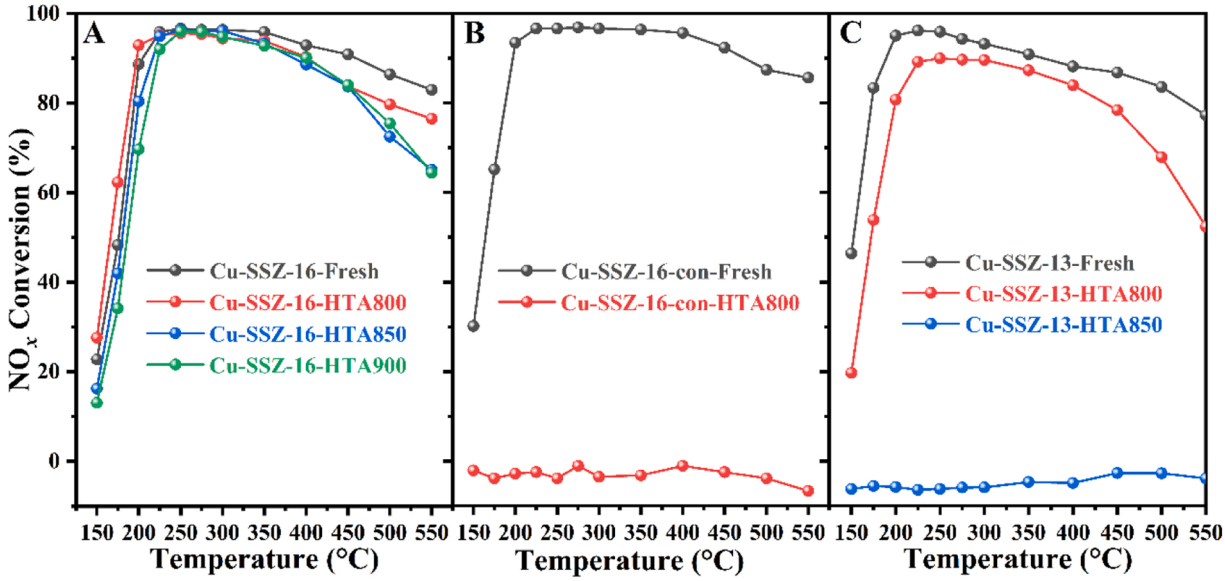

Fig. 6. NO_x conversion as a function of temperature in NH_3-SCR reaction over fresh and hydrothermally aged (A) Cu-SSZ-16, (B) Cu-SSZ-16-con, and (C) Cu-SSZ-13 catalysts. Feed composition: 500 ppm of NO, 500 ppm of NH_3, 5 % O_2, and 5 % H_2O balanced with N_2 (GHSV=200000 h^{-1}).

ratio and Cu loading.

The zeolite framework structures of fresh and hydrothermally aged Cu-SSZ-16 was examined by XRD, SEM, MAS NMR, and N_2 sorption measurements. As the XRD results shown in Fig. S8 and Table S4, hydrothermal aging at 800 °C caused a slight decrease of diffraction peak intensities of the Cu-SSZ-16, which remained about 89.4 % crystallinity, while the Al-rich Cu-SSZ-16-con almost lost its crystallinity (Fig. S9) for the complete loss of NO_x reduction efficiency. Although Cu-SSZ-13 maintained its typical structure with crystallinity of about 52.8 % at 800 °C, it totally collapsed after increasing the hydrothermal aging temperature to 850 °C (Fig. S10). Notably, the Cu-SSZ-16 still had 73.9 % crystallinity after hydrothermal aging at 850 °C and 58.5 % crystallinity even after increasing the aging temperature to 900 °C. In addition, in the SEM images of Cu-SSZ-16 before and after hydrothermal treatments at different temperatures, no obvious change for the dihexahedron morphology could be found (Fig. S11). Fig. S12 and Table S5 display the N_2 sorption isotherms and BET results of high Cu-SSZ-16 catalysts before and after hydrothermal treatments. Only subtle changes happed after hydrothermal aging at 800 and 850 °C. Increasing the aging temperature to 900 °C, the BET surface area and micropore volume of the sample were decreased to 477 m^2/g and 0.20 cm^3/g, respectively. These results evidence that the high silica SSZ-16 zeolite shows outstanding hydrothermal stability.

Furthermore, ^{27}Al and ^{29}Si MAS NMR techniques were carried out to determine the change in the local environment of Al and Si species before and after hydrothermal treatments, as shown in Fig. S13. ^{27}Al NMR spectra of Cu-SSZ-16 before and after hydrothermal treatments gave a peak at 57.2 ppm assigned to 4-coordinated aluminum species. In addition, a small peak at around 0 ppm assigned to extra-framework Al species appeared in the fresh Cu-SSZ-16 sample, which may be caused by calcination and ion-exchange process. However, there is no peak of extra-framework Al species observed in hydrothermally aged samples. This does not mean that dealumination did not occur during the hydrothermal treatments, but the portion of Al detached from the zeolite framework remains NMR silent, for the possible explanations that the detached Al stays adjacent to paramagnetic Cu sites, or the detached Al is in highly distorted and heterogeneous sites [13]. The corresponding ^{29}Si NMR spectra (Fig. S13B) displays that Si(2Si) species disappeared together with significant decreasing of Si(3Si) species after hydrothermal treatments, indicating the occurrence of dealumination that induced a slight decrease of NO_x conversion after hydrothermal aging.

4. Conclusion

High silica SSZ-16 zeolite with Si/Al ratio at 6.7 was efficiently synthesized from a designed small molecular Et_4Me_2-diquat-6 as the OSDA inspired by theoretical simulations. Owing to the high silica feature, Cu-SSZ-16 catalyst exhibits much higher hydrothermal stability than the conventional Al-rich Cu-SSZ-16-con and Cu-SSZ-13 with similar Si/Al ratio and Cu loading. Importantly, the high silica Cu-SSZ-16 catalyst shows superior NO_x convention even after hydrothermal treatment under extremely high temperature at 900 °C. The concept for rational synthesis of high silica SSZ-16 zeolite might offer an attractive route for developing Cu-based small-pore zeolites with suitable element composition as efficient and stable NH_3-SCR catalysts in the future.

CRediT authorship contribution statement

Shichao Han: Investigation, Formal analysis, Writing – original draft. **Wei Rao** and **Xiaomin Tang:** Software, Writing – original draft. **Junyi Hu, Ye Ma** and **Yanhang Ma:** Data curation, Writing – review & editing. **Jinpeng Du** and **Zhongqi Liu:** Data curation. **Xiangju Meng** and **Qinming Wu:** Formal analysis. **Wenpo Shan, Feng-shou Xiao** and **Hong He:** Conceptualization, Methodology, Writing – review & editing. **Shichao Han, Wei Rao** and **Junyi Hu** contributed equally.

Declaration of Competing Interest

The authors declare that they have no known competing financial interests or personal relationships that could have appeared to influence the work reported in this paper.

Data availability

Data will be made available on request.

Acknowledgements

This work was supported by the National Natural Science Foundation of China (52225004, 51978640), the National Key R&D Program of China (2022YFC3701804, 2022YFA1506000), and the Science and Technology Innovation “2025” Major Program in Ningbo (2020Z103). We thank Shanghai Science and Technology Plan (21DZ2260400), ChEM (#EM02161943), SPST of ShanghaiTech University and the SPST Analytical Center at ShanghaiTech University.

Appendix A. Supporting information

Supplementary data associated with this article can be found in the online version at doi:10.1016/j.apcatb.2023.122746.

References

[1] M. Dusselier, M.E. Davis, Small-pore zeolites: synthesis and catalysis, Chem. Rev. 118 (2018) 5265–5329.
[2] T. Ryu, N.H. Ahn, S. Seo, J. Cho, H. Kim, D. Jo, G.T. Park, P.S. Kim, C.H. Kim, E. L. Bruce, P.A. Wright, I.-S. Nam, S.B. Hong, Fully copper-exchanged high-silica LTA zeolites as unrivaled hydrothermally stable NH_3-SCR catalysts, Angew. Chem. 129 (2017) 3304–3308.
[3] Y. Wang, T. Nishitoba, Y. Wang, X. Meng, F.-S. Xiao, W. Zhang, B. Marler, H. Gies, D. De Vos, U. Kolb, M. Feyen, R. McGuire, A.-N. Parvulescu, U. Müller, T. Yokoi, Cu-exchanged CHA-type zeolite from organic template-free synthesis: an effective catalyst for NH_3-SCR, Ind. Eng. Chem. Res. 59 (2020) 7375–7382.
[4] M. Chen, J. Li, W. Xue, S. Wang, J. Han, Y. Wei, D. Mei, Y. Li, J. Yu, Unveiling secondary-ion-promoted catalytic properties of Cu-SSZ-13 zeolites for selective catalytic reduction of NOx, J. Am. Chem. Soc. 144 (2022) 12816–12824.
[5] D. Xie, L.B. McCusker, C. Baerlocher, S.I. Zones, W. Wan, X. Zou, SSZ-52, a zeolite with an 18-layer aluminosilicate framework structure related to that of the DeNOx catalyst Cu-SSZ-13, J. Am. Chem. Soc. 135 (2013) 10519–10524.
[6] J. Kim, S.J. Cho, D.H. Kim, Facile synthesis of KFI-type zeolite and its application to selective catalytic reduction of NOx with NH_3, ACS Catal. 7 (2017) 6070–6081.
[7] L. Han, S. Cai, M. Gao, J. Hasegawa, P. Wang, J. Zhang, L. Shi, D. Zhang, SelectiVe Catalytic Reduction of NOx with NH_3 by using novel catalysts: state of the art and future prospects, Chem. Rev. 119 (2019) 10916–10976.
[8] Y. Shan, J. Du, Y. Zhang, W. Shan, X. Shi, Y. Yu, R. Zhang, X. Meng, F.-S. Xiao, H. He, Selective catalytic reduction of NOx with NH_3: opportunities and challenges of Cu-based small-pore zeolites, Natl. Sci. Rev. (2021) nwab010.
[9] C. Liu, G. Malta, H. Kubota, T. Toyao, Z. Maeno, K. Shimizu, Mechanism of NH_3-selective catalytic reduction (SCR) of NO/NO_2 (Fast SCR) over Cu-CHA *in situ/operando* infrared spectroscopy and density functional theory, J. Phys. Chem. C. 125 (2021) 21975–21987.
[10] Q. Ye, L. Wang, R.T. Yang, Activity, propene poisoning resistance and hydrothermal stability of copper exchanged chabazite-like zeolite catalysts for SCR of NO with ammonia in comparison to Cu/ZSM-5, Appl. Catal. A Gen. 427–428 (2012) 24–34.
[11] F. Giordanino, P.N.R. Vennestrøm, L.F. Lundegaard, F.N. Stappen, S. Mossin, P. Beato, S. Bordiga, C. Lamberti, Characterization of Cu-exchanged SSZ-13: a comparative FTIR, UV-Vis, and EPR study with Cu-ZSM-5 and Cu-β with similar Si/Al and Cu/Al ratios, Dalton Trans. 42 (2013) 12741–12761.
[12] D. Wang, Y. Jangjou, Y. Liu, M.K. Sharma, J. Luo, J. Li, K. Kamasamudram, W. S. Epling, A comparison of hydrothermal aging effects on NH_3-SCR of NOx over Cu-SSZ-13 and Cu-SAPO-34 catalysts, Appl. Catal. B 165 (2015) 438–445.
[13] J. Song, Y. Wang, E.D. Walter, N.M. Washton, D. Mei, L. Kovarik, M.H. Engelhard, S. Prodinger, Y. Wang, C.H.F. Peden, F. Gao, Toward rational design of Cu/SSZ-13 selective catalytic reduction catalysts: implications from atomic-level understanding of hydrothermal stability, ACS Catal. 7 (2017) 8214–8227.
[14] R. Villamaina, S. Liu, I. Nova, E. Tronconi, M.P. Ruggeri, J. Collier, A. York, D. Thompsett, Speciation of Cu cations in Cu-CHA catalysts for NH_3-SCR: effects of SiO_2/AlO_3 ratio and Cu-loading investigated by transient response methods, ACS Catal. 9 (2019) 8916–8927.
[15] C.H.F. Peden, Cu/Chabazite catalysts for ‘Lean-Burn’ vehicle emission control, J. Catal. 373 (2019) 384–389.
[16] H. Xu, W. Chen, Q. Wu, C. Lei, J. Zhang, S. Han, L. Zhang, Q. Zhu, X. Meng, D. Dai, S. Maurer, A.-N. Parvulescu, U. Müller, W. Zhang, T. Yokoi, X. Bao, B. Marler, D.E.

D. Vos, U. Kolb, A. Zheng, F.-S. Xiao, Transformation synthesis of aluminosilicate SSZ-39 zeolite from ZSM-5 and beta zeolite, J. Mater. Chem. A 7 (2019) 4420–4425.
[17] M. Moliner, C. Franch, E. Palomares, M. Grill, A. Corma, Cu-SSZ-39, an active and hydrothermally stable catalyst for the selective catalytic reduction of NOx, Chem. Commun. 48 (2012) 8264–8266.
[18] P. Xiao, Y. Wang, Y. Lu, T. De Baerdemaeker, A.-N. Parvulescu, U. Müller, D. De Vos, X. Meng, F.-S. Xiao, W. Zhang, B. Marler, U. Kolb, H. Gies, T. Yokoi, Effects of Al distribution in the Cu-exchanged AEI zeolites on the reaction performance of continuous direct conversion of methane to methanol, Appl. Catal. B 325 (2023), 122395.
[19] D. Jo, T. Ryu, G.T. Park, P.S. Kim, C.H. Kim, I.-S. Nam, S.B. Hong, Synthesis of high-silica LTA and UFI zeolites and NH_3-SCR performance of their copper-exchanged form, ACS Catal. 6 (2016) 2443–2447.
[20] S.T. Wilson, N.K. McGuire, C.S. Blackwell, C.A. Bateman, R.M. Kirchner, Synthesis, characterization, and structure of SAPO-56, a new member of the abc double-six ring family of materials with stacking sequence AABBCCBB, Stud. Surf. Sci. Catal. 98 (1995) 9–10.
[21] R.F. Lobo, S.I. Zones, R.C. Medrud, Synthesis and Rietveld refinement of the small-pore zeolite SSZ-16, Chem. Mater. 8 (1996) 2409–2411.
[22] D.W. Fickel, R.F. Lobo, Copper coordination in Cu-SSZ-13 and Cu-SSZ-16 investigated by variable-temperature XRD, J. Phys. Chem. C 114 (2010) 1633–1640.
[23] P. Zhao, B. Boekfa, K. Shimizu, M. Ogura, M. Ehara, Selective catalytic reduction of NO with NH_3 over Cu-exchanged CHA, GME, and AFX zeolites: a density functional theory study, Catal. Sci. Technol. 11 (2021) 1780–1790.
[24] D.W. Fickel, E. D'Addio, J.A. Lauterbach, R.F. Lobo, The ammonia selective catalytic reduction activity of copper-exchanged small-pore zeolites, Appl. Catal. B 102 (2011) 441–448.
[25] R. Li, X. Jiang, J. Lin, Z. Zhang, Q. Huang, G. Fu, Y. Zhu, J. Jiang, Understanding the influence of hydrothermal treatment on NH_3-SCR of NOx activity over Cux-SSZ-16, Chem. Eng. J. 441 (2022) 136021–136031.
[26] H. Kubota, C. Liu, T. Toyao, Z. Maeno, M. Ogura, N. Nakazawa, S. Inagaki, Y. Kubota, K. Shimizu, Formation and reactions of NH_4NO_3 during transient and steady-state NH_3-SCR of NOx over H-AFX zeolites: spectroscopic and theoretical studies, ACS Catal. 10 (2020) 2334–2344.
[27] A. Chokkalingam, W. Chaikittisilp, K. Iyoki, S.H. Keoh, Y. Yanaba, T. Yoshikawa, T. Kusamoto, T. Okubo, T. Wakihara, Ultrafast synthesis of AFX-Type zeolite with enhanced activity in the selective catalytic reduction of NOx and hydrothermal stability, RSC Adv. 9 (2019) 16790–16796.
[28] T. Yoshioka, K. Iyoki, Y. Hotta, Y. Kamimura, H. Yamada, Q. Han, T. Kato, C.A. J. Fisher, Z. Liu, R. Ohnishi, Y. Yanaba, K. Ohara, Y. Sasaki, A. Endo, T. Takewaki, T. Sano, T. Okubo, T. Wakihara, Dealumination of small-pore zeolites through pore-opening migration process with the aid of pore-filler stabilization, Sci. Adv. 8 (2022), eabo3093.
[29] R.H. Archer, S.I. Zones, M.E. Davis, Imidazolium structure directing agents in zeolite synthesis: Exploring guest/host relationships in the synthesis of SSZ-70, Microporous Mesoporous Mater. 130 (2010) 255–265.
[30] N. Martín, C. Paris, P.N.R. Vennestrøm, J.R. Thøgersen, M. Moliner, A. Corma, Cage-based small-pore catalysts for NH_3-SCR prepared by combining bulky organic structure directing agents with modified zeolites as reagents, Appl. Catal. B 217 (2017) 125–136.
[31] A. Turrina, R. Garcia, P.A. Cox, J.L. Casci, P.A. Wright, Retrosynthetic co-templating method for the preparation of silicoaluminophosphate molecular sieves, Chem. Mater. 28 (2016) 4998–5012.
[32] Q. Wu, H. Luan, F.-S. Xiao, Targeted synthesis of zeolites from calculated interaction between zeolite structure and organic template, Natl. Sci. Rev. (2022), nwac023.
[33] D. Schwalbe-Koda, S. Kwon, C. Paris, E. Bello-Jurado, Z. Jensen, E. Olivetti, T. Willhammar, A. Corma, Y. Román-Leshkov, M. Moliner, R. Gómez-Bombarelli, A priori control of zeolite phase competition and intergrowth with high-throughput simulations, Science 374 (2021) 308–315.
[34] Database of Zeolite Structures. http://www.iza-structure.org/databases/.
[35] S.L. Mayo, B.D. Olafson, W.A. Goddard, DREIDING: a generic force field for molecular simulations, J. Phys. Chem. 94 (1990) 8897–8909.
[36] J.D. Gale, A.L. Rohl, The general utility lattice program (GULP), Mol. Simul. 29 (2003) 291–341.
[37] R. Pophale, F. Daeyaert, M.W. Deem, Computational prediction of chemically synthesizable organic structure directing agents for zeolites, J. Mater. Chem. A 1 (2013) 6750–6760.
[38] M.J. Frisch, G.W. Trucks, H.B. Schlegel, Gaussian 09, Revision B.01, Gaussian, Inc., Wallingford, CT, (2010).
[39] T. Lu, F. Chen, Quantitative analysis of molecular surface based on improved Marching Tetrahedra algorithm, J. Mol. Graph. Model 38 (2012) 314–323.
[40] T. Lu, F. Chen, Multiwfn: A multifunctional wavefunction analyzer, J. Comput. Chem. 33 (2012) 580–592.
[41] S.I. Zones, Conversion of faujasites to high-silica chabazite SSZ-13 in the presence of N,N,N-trimethyl-1-adamantammonium iodide, J. Chem. Soc. Faraday Trans. 87 (1991) 3709–3716.
[42] P. Sun, Q. Jin, L. Wang, B. Li, D. Ding, A study on the templating ability of diquaternary cations for the zeolite synthesis in terms of energetics, J. Porous Mater. 10 (2003) 145–150.
[43] B. Han, S.-H. Lee, C.-H. Shin, P.A. Cox, S.B. Hong, Zeolite synthesis using flexible diquaternary alkylammonium ions $(C_nH_{2n+1})_2HN^+(CH_2)_5N^+H(C_nH_{2n+1})_2$ with n = 1−5 as structure-directing agents, Chem. Mater. 17 (2005) 477–486.
[44] P. Lu, S. Ghosh, M. Dorneles de Mello, H.S. Kamaluddin, X. Li, G. Kumar, X. Duan, M. Abeykoon, J.A. Boscoboinik, L. Qi, H. Dai, T. Luo, S. Al-Thabaiti, K. Narasimharao, Z. Khan, J.D. Rimer, A.T. Bell, P. Dauenhauer, K.A. Mkhoyan, M. Tsapatsis, Few-unit-cell MFI zeolite synthesized using a simple di-quaternary ammonium structure-directing agent, Angew. Chem. Int. Ed. 60 (2021) 19214–19221.
[45] J.R. Di Iorio, R. Gounder, Controlling the isolation and pairing of aluminum in chabazite zeolites using mixtures of organic and inorganic structure-directing agents, Chem. Mater. 28 (2016) 2236–2247.
[46] L.D. Rollmann, J.L. Schlenker, S.L. Lawton, C.L. Kennedy, G.J. Kennedy, D. J. Doren, On the role of small amines in zeolite synthesis, J. Phys. Chem. B 103 (1999) 7175–7183.
[47] K.H. Møller, M. Debost, L. Lakiss, S. Kegnæs, S. Mintova, Interzeolite conversion of a micronsized FAU to a nanosized CHA zeolite free of organic structure directing agent with a high CO_2 capacity, RSC Adv. 10 (2020) 42953–42959.
[48] C.-R. Boruntea, G. Sastre, L.F. Lundegaard, A. Corma, P.N.R. Vennestrøm, Synthesis of high-silica erionite driven by computational screening of hypothetical zeolites, Chem. Mater. 31 (2019) 9268–9276.
[49] T. Yoshioka, Z. Liu, K. Iyoki, A. Chokkalingam, Y. Yonezawa, Y. Hotta, R. Ohnishi, T. Matsuo, Y. Yanaba, K. Ohara, T. Takewaki, T. Sano, T. Okubo, T. Wakihara, Ultrafast and continuous-flow synthesis of AFX zeolite via interzeolite conversion of FAU zeolite, React, Chem. Eng. 6 (2021) 74–81.
[50] Z. Liu, A. Chokkalingam, S. Miyagi, T. Sano, T. Okubo, Revealing scenarios of interzeolite conversion from FAU to AEI through the variation of starting materials, Phys. Chem. Chem. Phys. 19 (2017) 73–81.
[51] J.H. Lee, M.B. Park, J.K. Lee, H.-K. Min, M.K. Song, S.B. Hong, Synthesis and characterization of ERI-type UZM-12 zeolites and their methanol-to-olefin performance, J. Am. Chem. Soc. 132 (2010) 12971–12982.
[52] Z. Zhu, H. Xu, B. Wang, J. Yin, J. Jiang, H. Lü, P. Wu, Intensified interzeolite transformation: ultrafast synthesis of active and stable Ti-Beta zeolites without solvents, Chem. Commun. 55 (2019) 14279–14282.
[53] H. Baraǹska, B. Czerwiǹska, A. Łabudziǹska, Raman spectroscopic study of zeolite ZSM-5, Synth., J. Mol. Struct. 143 (1986) 485–488.
[54] P.K. Dutta, D.C. Shieh, M. Puri, Raman spectroscopic study of the synthesis of zeolite Y, J. Phys. Chem. 91 (1987) 2332–2336.
[55] F. Fan, Z. Feng, G. Li, K. Sun, P. Ying, C. Li, In situ UV Raman spectroscopic studies on the synthesis mechanism of zeolite X, Chem. Eur. J. 14 (2008) 5125–5129.
[56] J. Zhang, Y. Chu, F. Deng, Z. Feng, X. Meng, F.-S. Xiao, Evolution of D6R units in the interzeolite transformation from FAU, MFI or *BEA into AEI: transfer or reassembly? Inorg. Chem. Front. 7 (2020) 2204–2211.
[57] Y. Sada, A. Chokkalingam, K. Iyoki, M. Yoshioka, T. Ishikawa, Y. Naraki, Y. Yanaba, H. Yamada, K. Ohara, T. Sano, T. Okubo, Z. Liu, T. Wakihara, Tracking the crystallization behavior of high-silica FAU during AEI-type zeolite synthesis using acid treated FAU-type zeolite, RSC Adv. 11 (2021) 23082–23089.
[58] S.I. Zones, Conversion of faujasites to high-silica chabazite SSZ-13 in the presence of N,N,N-trimethyl-1-adamantammonium iodide, J. Chem. Soc. Faraday Trans. 87 (1991) 3709–3716.